Hindawi Publishing Corporation
Journal of Nanomaterials
Volume 2015, Article ID 745312, 9 pages
http://dx.doi.org/10.1155/2015/745312

Research Article

Experimental Study and Stabilization Mechanisms of Silica Nanoparticles Based Brine Mud with High Temperature Resistance for Horizontal Shale Gas Wells

Xian-yu Yang, Ye Yue, Ji-hua Cai, Yue Liu, and Xiao-ming Wu

School of Engineering, China University of Geosciences, Wuhan 430074, China

Correspondence should be addressed to Ji-hua Cai; catchercai@hotmail.com

Received 22 July 2015; Revised 10 October 2015; Accepted 12 October 2015

Academic Editor: Sesha Srinivasan

Previous studies showed that silica nanoparticles based fresh water drilling muds had good thermal stability up to 160°C; however its performance at high salt concentration was rather poor. Therefore, high performance silica nanoparticles based brine mud (NPBMs) with high temperature resistance for horizontal shale gas wells was proposed. Thermal stability tests from ambient temperature to 180°C, along with pressure transmission tests and rheology analysis, were performed to evaluate comprehensive properties of the NPBMs. Results show that the NPBMs embody excellent salt tolerance and thermal resistance for their rheological parameters did not suffer significant fluctuation. Fluid loss of the NPBM-1 (4% NaCl plus 3% KCl) at 180°C was only 7.6 mL while the NPBM-2 (10% NaCl plus 3% KCl) had a fluid loss of 6.6 mL at 150°C. Low water activity and good lubricity of the NPBMs were beneficial to improve wellbore stability and reduce friction resistance. Pressure transmission tests on the NPBM-1 show that it can mitigate or even prevent the transmission of drilling mud pressure into shale thus improving wellbore stability. Additionally, optimal rheological models for the NPBM-1 and the NPBM-2 were Herschel-Bulkley model and Power Law model separately.

1. Introduction

Fluid penetration from water-based drilling mud into shale formations results in swelling and subsequent wellbore instability. Shale accounts for 75% of all footage drilled and is responsible for 90% of wellbore stability problems [1–3]. Maintaining wellbore stability is one of the most critical aspects of oil and gas drilling. The main cause of shale instability for both soft and hard shale is water absorption and subsequent swelling and sloughing of the wellbore [4]. Wellbore pressure penetrates into the pore space when water invades into the shale. This reduction of true overbalance, which acts like a support pressure for the hole, can result in shale failure and wellbore instability [5].

It is generally accepted that balanced activity oil-continuous mud offers a good solution to shale instability problems since there is no interaction between oil and shale [4]. However, for environmental and economic considerations, water-based mud would be much preferred if the interaction between drilling mud and shale could be minimized. Hayatdavoudi and Apande [6] found that the best possible way of preventing contact between argillaceous rock and water is to seal off exposed clayey surfaces. Carminati et al. [7] showed that the most effective additives in controlling the pore fluid pressure in the formation and the shale hardness, and consequently in preventing shale instability, are the silicates. Pore blocking is a time dependent process that requires a few hours to develop. Van Oort et al. [3] introduced silicate-based mud as superior fluids for drilling troublesome formations like intact and (micro)fractured shale and chalks. In addition, these inorganic systems are environmentally friendly and inexpensive. Reid et al. [8] regarded the interaction between potassium ions and polyols at the clay surface as the critical factor in the provision of shale inhibition. Zhong et al. [9] elaborated the mechanisms of polyether diamine to improve shale wellbore stability in water-based drilling fluids.

Different from traditional sandstone or carbonate reservoirs, shale from China and North America is featured with nanosized pores. The pore diameter of gas shale in China and North America is in a range of 5–300 nm and 8–100 nm separately [10–16]. Therefore, only nanoparticles

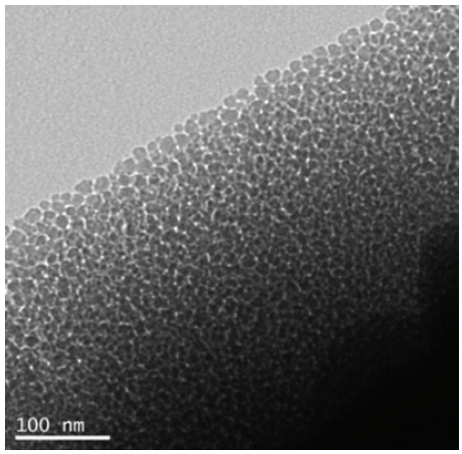

Figure 1: TEM picture of nano-SiO_2 dispersion.

have the possibility of plugging pore throats in shale. On the other side, Cai et al. [17], Sharma et al. [18], Akhtarmanesh et al. [19], Kapadnis et al. [20], and Liang et al. [21] found that wellbore stability of shale could be improved with nanoparticles. For shale gas wells, especially the ones with long intervals, good cutting transferring capability, excellent inhibition on shale to absorb water, and good lubricity to decrease circulating friction resistance become the focuses of designing inhibitive drilling mud.

Our previous studies have showed that silica nanoparticles (nano-SiO_2) based fresh water mud could improve wellbore stability of shale and had good thermal stability up to 160°C [17, 22]. However, its performance at high salt concentration was rather poor as the American Petroleum Institute (API) filtration was over 15 mL at 120°C. In this paper, basing on synergic wellbore stabilization theory of physical plugging of nanoparticles, balanced activity with inorganic salts, chemical inhibition, and rational mud density, high performance silica nanoparticles (nano-SiO_2) based brine mud (NPBMs) with high temperature resistance for horizontal shale gas wells was proposed. The thermal stability tests on rheology, filtration, lubricity, and water activity of the NPBMs from ambient temperature to 180°C were carried out and pressure transmission tests were run to systematically evaluate the performances of the NPBMs. In addition, rheological model of the NPBMs was also analyzed.

2. Material and Methods

2.1. Material

2.1.1. Nanoparticles. Nano-SiO_2 used in this study was milky white dispersion and had a concentration of 30%. It was procured from Nanjing Haitai Nano Materials Co., Ltd., China. Its transmission electron microscopy (TEM) picture is shown in Figure 1. The diameter of nano-SiO_2 ranges between 10 nm and 20 nm.

2.1.2. Shale Properties. Shale is a sedimentary rock that mineralogically consists of clays, quartz, and other silicate and carbonate minerals. Because of its high clay content, shale tends to absorb water from water-based mud, which results in swelling and sloughing of the wellbore. In this study, core samples from the first shale gas well of Jiangxi, China, were obtained. The mineralogical composition of this shale is listed in Table 1. It contains 45% clay minerals (25% chlorite plus 20% illite) showing strong water sensitivity and moderate brittleness.

Table 1: Composition of shale samples from the first shale gas well of Jiangxi, China.

X-ray diffraction	wt/%
Chlorite	25
Illite	20
Calcite	15
Feldspar	10
Gypsum	3
Pyrite	5
Quartz	22

2.1.3. Mud Used. The NPBMs with high temperature resistance were developed through basic formula optimization. A 4% NaCl brine mud and 10% NaCl brine mud were obtained separately. Both mud types contain clay (1.5% attapulgite, 1.5% sodium bentonite), nanoparticles (2% nano-SiO_2), fluid loss additives (0.3% LV-CMC, 1% Dristemp, and 2% lockseal), shale inhibitors (3% KL, 3% SPNH, 2% Soltex, 2% SMP-II, and 3% KCl), pH regulator (Na_2CO_3), and weighting material (10% $BaSO_4$). The concentration of $BaSO_4$ could also be adjusted according to the pore pressure of the formation. The 4% NaCl and 10% NaCl NPBM contained 0.14% Na_2CO_3 and 0.2% Na_2CO_3 separately and were denoted as NPBM-1 and NPBM-2. Among the additives used, attapulgite was bought from Anhui Mingyuan New Material Co., Ltd., China. Sodium bentonite was supplied by Weifang Huixin Bentonite Co., Ltd., Shandong, China. LV-PAC, SPNH, KL, and SMP-II were offered by East Zhengzhou Drilling Additive Co., Ltd., China. Dristemp and Soltex were supplied by Chevron Phillips Chemical Company LP. NaCl, KCl, Na_2CO_3, and $BaSO_4$ were standard chemical reagents bought from Sinopharm Chemical Co. Ltd.

2.2. Experimental Methods

2.2.1. Thermal Stability Tests. The thermal stability tests consisted of heating the brine mud (BM) and the NPBMs to a given temperature from ambient temperature to 180°C for 16 h with OFITE roller oven and then cooling it to ambient temperature. The rheological properties were evaluated by a ZNN-D6 six-speed rotary viscometer. The readings at 600 rpm and 300 rpm could be marked as θ_{600} and θ_{300}, respectively. The plastic viscosity (PV) and yield point (YP) could be calculated according to the equations as follows:

$$\begin{aligned} \mathrm{PV} &= \theta_{600} - \theta_{300},\ \mathrm{mPa \cdot s} \\ \mathrm{YP} &= 0.5\left(2\theta_{300} - \theta_{600}\right),\ \mathrm{Pa}. \end{aligned} \tag{1}$$

The initial gel strength ($\tau_{10\,\mathrm{s}}$) and the final gel strength ($\tau_{10\,\mathrm{min}}$) of the BM and the NPBMs were also measured with the ZNN-D6 six-speed rotary viscometer.

Table 2: Rheological properties of BM with/without nanoparticles.

Formula	Temperature	PV (mPa·s)	YP (Pa)
BM-1	25°C	45	23
	120°C	67	31
	150°C	66	16.5
	180°C	63	17.5
BM-2	25°C	42	25
	120°C	57	32
	150°C	61	26
	180°C	51	23.5
NPBM-1	25°C	52	26
	120°C	66	32
	150°C	66	17
	180°C	76	22
NPBM-2	25°C	50	29
	120°C	67	32
	150°C	58	27
	180°C	47	20.5

Table 3: Gel strength of the BM with or without nanoparticles at elevated temperature.

Temperature	$\tau_{10\,s}/\tau_{10\,min}$ (Pa/Pa)			
	BM-1	BM-2	NPBM-1	NPBM-2
25°C	2/6	1.5/4	2.5/8	2.1/6
120°C	1.5/2.5	1.5/2.5	1.6/2.6	1.6/2.6
150°C	2.5/7.5	2.5/6	2.4/5	2/4
180°C	2.5/4	2.1/5.5	2/3.2	2/3.3

After that, the filtration properties of the NPBMs were tested for 30 minutes by a ZNS-5A moderate pressure filter press with a pressure difference of 0.69 MPa at ambient temperature (25°C). The friction coefficient was measured with EP-2 extreme pressure lubricity tester. The motor speed was adjusted to 60 rpm and the torque was loaded to 15.96 N·m. The test procedures followed the API standards. Novasina Labswift water activity tester was used to analyze the water activity of drilling mud. The results were shown in Tables 2 and 3 and Figures 2–5.

2.2.2. High Temperature and High Pressure (HTHP) Rheological Tests. Fann 50SL rheometer was employed to evaluate the HTHP rheological properties at 5.17 MPa. The temperature range was set from 25°C to 180°C. The readings at 100 rpm of the rheometer were derived and the rheological curve was drawn, as shown in Figure 6.

2.2.3. Pressure Transmission Tests. The interaction between varied working fluids with shale was investigated by HKY-3 pressure transmission test apparatus. The shale samples used were collected from the first shale gas well of Jiangxi, China, and had similar original permeability. The confining pressure and upstream pressure were set as 3.5 MPa and 2.5 MPa separately while the initial downstream pressure was set as zero. The downstream pressure data was collected for the calculation of permeability (k) of shale sample in contact with working fluids. It was decided to first flow brine (10% NaCl) through shale samples until equilibrium was reached so as to produce saturated shale samples. For the second step, the test was run using compound brine (7% NaCl plus 3% KCl). In the third step, the test was run using the NPBM-1 at ambient temperature. To verify the capability of the NPBM-1 mitigating pressure penetration into shale, the upstream pressure was increased to 10 MPa in the last step. Table 4 and Figures 7 and 8 present the pressure penetration test results. A transient pressure model is used for calculating the permeability of shale sample [10]. Another similar pressure transmission tests were undergone with the difference that the NPBM-1 at ambient temperature was substituted by the NPBM-1 mud after hot roll at 180°C and being cooled to ambient temperature.

2.2.4. Rheological Model Analyses. Rheological model of the NPBMs have important and direct effect on the calculation of circulating pressure loss, pressure surge, cuttings carrying performances and water horse power of drilling bits which are beneficial to rapid drilling, borehole cleaning, and wellbore stabilization. A data processing system (DPS) software was used to analyze the rheological model of the NPBMs.

3. Results

3.1. Thermal Stability Tests

3.1.1. Rheology and Filtration. Table 2 and Figure 2 present the PV and YP of the NPBMs compared with non-NP mud. Standard deviation data has been also added in Figure 2. The addition of nano-SiO_2 does not show strong influence on the PV and YP of the BM. Up to 10 types of additives had been used; therefore linear increase or decrease of PV or YP did not appear (Figure 2). To the NPBM-1, it experienced an increase of 24 mPa·s for the PV with the increase of temperature, which can be attributed with the fact that high temperature may promote the hydration of sodium bentonite and increase the internal friction of the NPBM-1 with lower salinity (4% NaCl), thus increasing the PV. Its YP suffered a fluctuation from 17 Pa to 32 Pa, which is still acceptable to drilling engineering. Therefore, we conclude that its thermal tolerance is 180°C. To the NPBM-2, for its higher salinity (10% NaCl), its PY dropped about 20 mPa·s when the temperature increased from 120°C to 180°C. Taking its PV at 25°C as a referenced example, we deduce that its temperature tolerance is 150°C.

The initial gel strength ($\tau_{10\,s}$) and the final gel strength ($\tau_{10\,min}$) of BM mud with/without the addition of nano-SiO_2 were presented in Table 3. The presence of nanoparticles did not bring significant change to the bentonite mud and showed good compatibility.

Figure 3 shows the filtration properties of the NPBMs with the elevation of temperature. For the NPBM-1, the fluid loss was less than 7.6 mL at 180°C while, for the NPBM-2, the fluid loss was below 6.6 mL at 150°C. From 150°C to 180°C, the NPBM-2 experienced higher fluid loss which might be explained for its higher NaCl concentration (10%).

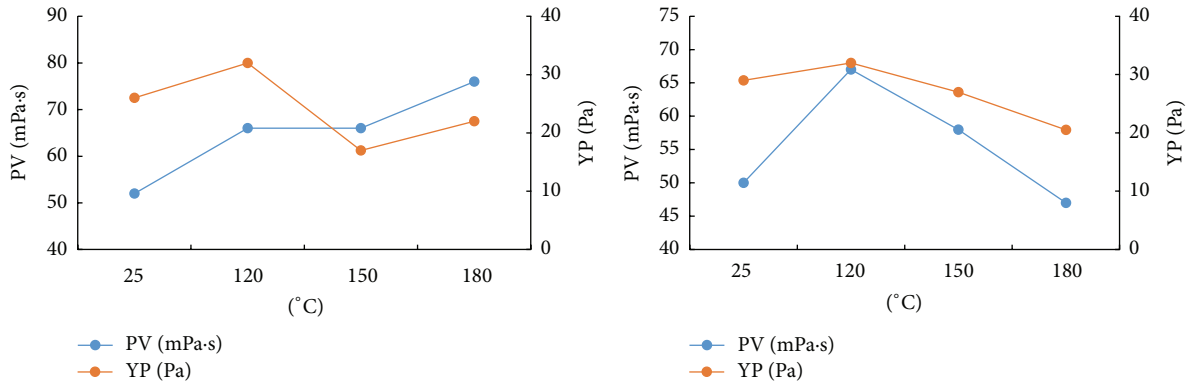

(a) NPBM-1 (b) NPBM-2

Figure 2: Change of plastic viscosity and yield point versus temperature.

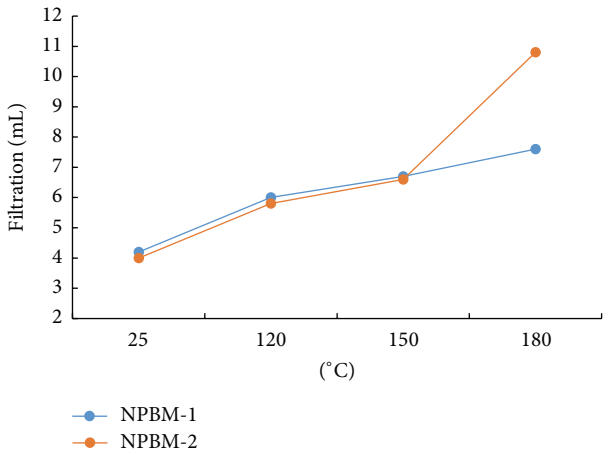

Figure 3: Change of fluid loss versus temperature.

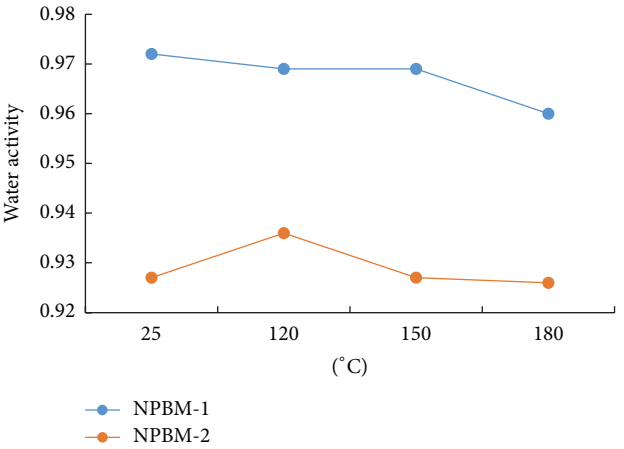

Figure 5: Change of water activity versus temperature.

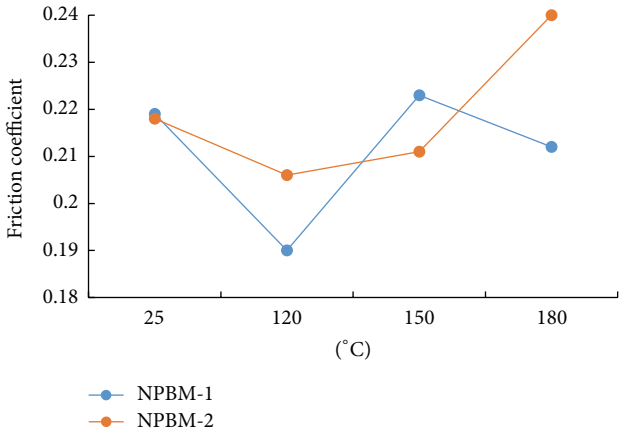

Figure 4: Change of friction factor versus temperature.

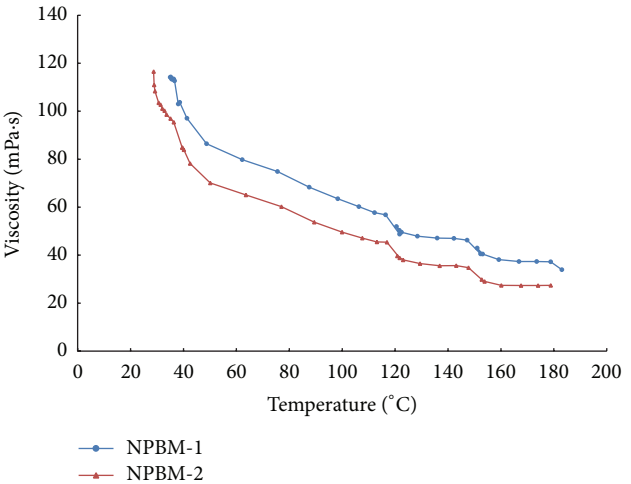

Figure 6: HTHP rheological curves of the NPBMs at 100 rpm.

By integrating Figures 2 and 3 and Tables 2 and 3 together, we found that the NPBMs show excellent properties at high salt concentration up to 13% and high temperature up to 180°C (NPBM-1) or 150°C (NPBM-2).

3.1.2. Lubricity and Water Activity. In the drilling of horizontal shale gas well with long interval, drilling contractors not only need to face with the technical problem of lost circulation and collapse but also need to reduce friction resistance and ensure the transferring of cuttings. From Figure 4, it is observed that the friction coefficient kept around 0.2 during the increasing of temperature from ambient temperature to

Table 4: Testing conditions and results of pressure transmission tests.

Number of shale samples	Testing fluid	Permeability (mD)	Reducing rate of permeability (%)	Testing conditions	Test time (h)
1#	10% NaCl	0.91	—	Upstream pressure: 2.3 MPa Downstream pressure: 0 MPa	3
	7% NaCl + 3% KCl	2.72×10^{-3}	99.7		30
	NPBM-1 at 25°C	1.96×10^{-6}	99.99		40
	NPBM-1 at 25°C	1.5×10^{-5}	99.99	Upstream pressure: 10 MPa Downstream pressure: 0.02 MPa	30
2#	10% NaCl	1.89	—	Upstream pressure: 2.3 MPa Downstream pressure: 0 MPa	3
	7% NaCl + 3% KCl	2.17×10^{-3}	99.89		30
	NPBM-1 after being rolled at 180°C	4.69×10^{-6}	99.99		60
	NPBM-1 after being rolled at 180°C	1.29×10^{-5}	99.99	Upstream pressure: 10 MPa Downstream pressure: 0.02 MPa	20

180°C, with fluctuation in a narrow range. Excellent lubricity performance is very beneficial for the reducing of friction resistance of drilling bits and tools.

Lower water activity is helpful to improve wellbore stability of shale to some extent [4]. Figure 5 presents water activity of the NPBMs from ambient temperature to 180°C. Water activity of the NPBM-1 and NPBM-2 was in the range of 0.96~0.972 and 0.926~0.936, respectively, indicating good thermal resistance. The NPBM-2 had lower water activity than the NPBM-2 for its higher NaCl concentration (10%).

3.2. HTHP Rheological Tests. As shown in Figure 6 both the NPBMs types endured a decrease of viscosity with the elevation of temperature. However, The NPBW-1 shows better thermal stability than the NPBW-2. It may be attributed to its lower salinity.

3.3. Pressure Transmission Tests. Pressure transmission tests are often used to study the transmission of drilling mud pressure to pore fluid pressure which has critical impact on wellbore stability issue [4, 5, 18, 24]. In this study, HKY-3 pressure transmission test apparatus was used to evaluate whether the NPBMs could mitigate the pressure transmission into shale or not. As shown in Table 1, the shale sample from the first shale gas well of Jiangxi, China, has 45% clay and 22% quartz, showing strong water sensitivity and moderate brittleness.

Table 4 and Figures 7 and 8 summarized the testing conditions and results of pressure transmission tests.

In the first step with brine containing 10% NaCl, the upstream pressure penetrated into the downstream fast in about 6 h and the permeability of the shale sample was derived as 0.91 mD, as shown in Table 4 and Figure 7. Then the 10% NaCl was substituted by a compound brine (7% NaCl plus 3% KCl), the upstream pressure penetrated fast into the downstream in about 30 h, and the permeability of the shale sample was derived as 2.72×10^{-3} mD. Compound brine shows much more inhibition effect on the shale sample. After that, the compound brine was substituted by the NPBM-1 and the downstream pressure curve kept flat in about 40 h which shows that the NPBM-1 can mitigate or even prevent the

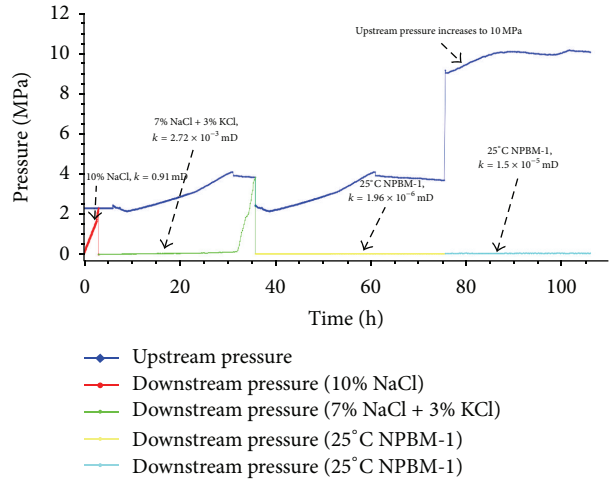

Figure 7: Pressure transmission test curves of the shale with brine and the NPBM-1 at ambient temperature.

transmission of upstream pressure (simulated drilling mud pressure). The calculated permeability of the shale sample was 1.96×10^{-6} mD (or 1.96 nD) and the reducing rate of shale permeability compared with brine was 99.99%. To confirm the inhibition effect, the upstream pressure was increased from 3.5 MPa to 10 MPa (Figure 7), the downstream pressure still kept constant for 30 h, and the calculated permeability of the shale was lower as 1.5×10^{-5} mD (or 15 nD). The permeability of shale sample in contact with NPBM-1 at ambient temperature is less than thousandth of the permeability of shale sample with compound brine. Shale permeability decreased from the level of milli-Darcy (mD) to the level of nano-Darcy (nD) showing that the invasion of water from drilling mud into shale sample was restricted to a great extent.

Another similar pressure transmission tests were undergone with the difference that the NPBM-1 at ambient temperature was substituted by the NPBM-1 mud after hot roll at 180°C and being cooled to ambient temperature. The results were shown in Figure 8. In the first step with brine (10% NaCl), similar result was observed to the above and the

Table 5: Rheological equation fitting in different temperature of NPBM-1.

Flow pattern	Determination coefficient (R^2), test value (F), and significant level (p)			
	25°C	120°C	150°C	180°C
Bingham	$\tau = 10.431 + 0.073 \times \gamma$ $R^2 = 0.9557$, $F = 86.26$, $p = 0.007$	$\tau = 10.758 + 0.094 \times \gamma$ $R^2 = 0.9578$, $F = 90.69$, $p = 0.007$	$\tau = 5.905 + 0.080 \times \gamma$ $R^2 = 0.9856$, $F = 273.02$, $p = 0.001$	$\tau = 9.787 + 0.093 \times \gamma$ $R^2 = 0.9757$, $F = 273.02$, $p = 0.001$
Power Law	$\tau = 1.440 \times \gamma^{0.579}$ $R^2 = 0.9995$, $F = 8414.51$, $p = 0.000$	$\tau = 1.239 \times \gamma^{0.635}$ $R^2 = 0.9919$, $F = 489.93$, $p = 0.000$	$\tau = 0.504 \times \gamma^{0.740}$ $R^2 = 0.9994$, $F = 7004.41$, $p = 0.000$	$\tau = 0.990 \times \gamma^{0.665}$ $R^2 = 0.9978$, $F = 1827.63$, $p = 0.000$
Carson	$\tau^{1/2} = 3.6146^{1/2} + 0.054^{1/2} \times \gamma^{1/2}$ $R^2 = 0.9874$, $F = 313.75$, $p = 0.001$	$\tau^{1/2} = 3.304^{1/2} + 0.072^{1/2} \times \gamma^{1/2}$ $R^2 = 0.9868$, $F = 298.52$, $p = 0.001$	$\tau^{1/2} = 1.378^{1/2} + 0.067^{1/2} \times \gamma^{1/2}$ $R^2 = 0.9959$, $F = 982.74$, $p = 0.000$	$\tau^{1/2} = 3.099^{1/2} + 0.071^{1/2} \times \gamma^{1/2}$ $R^2 = 0.9943$, $F = 702.67$, $p = 0.000$
Herschel-Bulkley	$\tau = 1.463 + 1.178 \times \gamma^{0.606}$ $R^2 = 1$, $F = 31230$, $p = 0.000$	$\tau = 1.356 + 1.064 \times \gamma^{0.656}$ $R^2 = 0.9922$, $F = 190.19$, $p = 0.007$	$\tau = 1.181 + 0.420 \times \gamma^{0.764}$ $R^2 = 0.9998$, $F = 7393.42$, $p = 0.000$	$\tau = 2.447 + 0.733 \times \gamma^{0.706}$ $R^2 = 0.9988$, $F = 1277.66$, $p = 0.000$

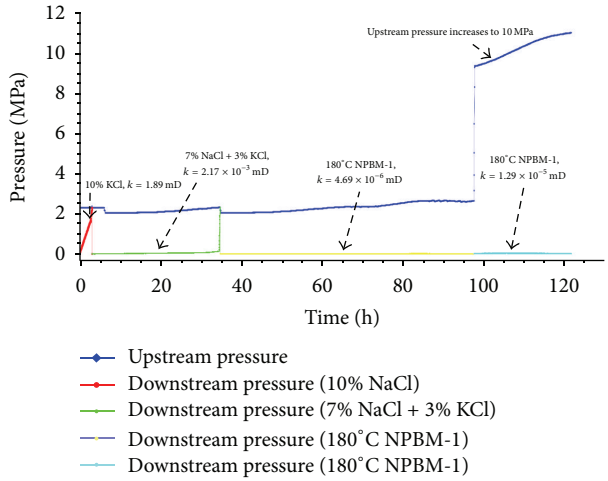

Figure 8: Pressure transmission test curves of the shale with brine and the NPBM-1 after being rolled at 180°C.

calculated permeability was 1.89 mD. Then the 10% NaCl was substituted by the compound brine (7% NaCl + 3% KCl), the upstream pressure penetrated fast into the downstream in about 30 h, and the permeability of the shale sample was derived as 2.12×10^{-3} mD. Compound brine still played well than 10% NaCl. After that, the compound brine was substituted by the NPBM-1 after being rolled at 180°C and the downstream pressure still kept flat in about 60 h and the permeability obtained was 4.69×10^{-6} mD (or 4.69 nD). The decreasing rate of shale permeability was as high as 99.99%. Similarly, with the upstream pressure being risen to 10 MPa again, the downstream pressure almost kept constant for 20 h and the calculated permeability of the shale was lower as 1.29×10^{-5} mD (or 12.9 nD). It indicates that, even after hot roll at 180°C, the NPBM-1 still shows excellent capability to mitigate or prevent the penetration of pressure from drilling fluid into the shale sample.

From Figures 7 and 8, we can see that although compound brine shows better inhibitive effect on the shale sample compared with 10% NaCl, the NPBM-1 could embody much more inhibition effect on the shale samples and thus improve wellbore stability, either at ambient temperature or after being rolled at 180°C.

3.4. Rheological Model Analysis with DPS Software. The investigation of rheological model analysis is to study the relationship of shearing stress (τ) and shearing velocity (γ). In the regression process with DPS software, determination coefficient (R^2), test value (F), and significant level (p) were adopted to evaluate regression precision of different flow models. Results show that the optimal rheological models for the NPBM-1 and NPBM-2 were Herschel-Bulkley model and Power Law model separately.

In the fitting process, the optimal rheological model was chosen according to the coefficient of determination (R^2), the test value (F), and the significant level (p). High value of R^2 and F indicate that the observed value and the fitting value are closer, and it means that the dispersion of the point is relatively close to the curve from the whole point of view. The significant level (p) is considered as arithmetic root of residual sum of squares. Naturally, the fitting equation with smaller p is accurate so the p gives a measure of the deviation from the observation point and the regression curve.

With comprehensive consideration of R^2, F, and p together, as shown in Tables 5 and 6, the optimal rheological models for the NPBM-1 and NPBM-2 were Herschel-Bulkley model and Power Law model, separately.

4. Discussion of the Mechanisms of the NPBMs

In this section, the mechanics of the NPBMs were discussed in detail.

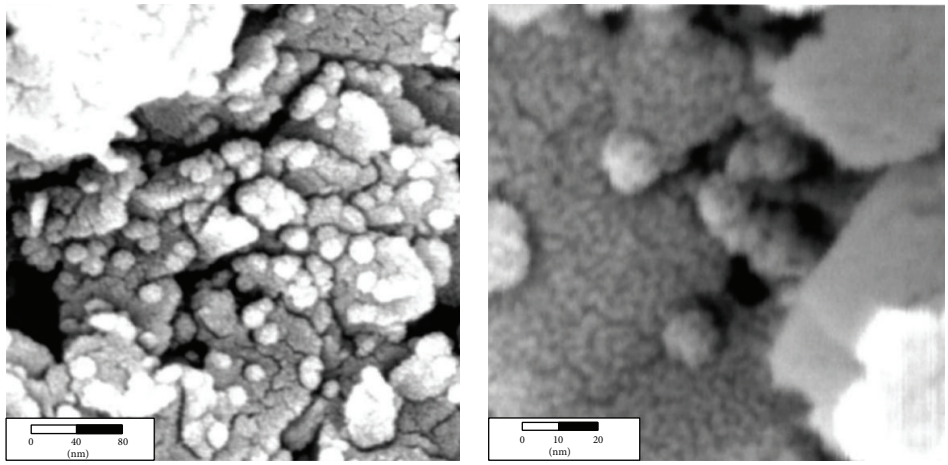

(a) Magnified 80000 times (b) Magnified 200000 times

Figure 9: SEM picture of plugging shale using nano-SiO_2 [23].

Table 6: Rheological Equation fitting in different temperature of NPBM-2.

Flow pattern	Determination coefficient (R^2), test value (F), and significant level (p)			
	25°C	120°C	150°C	180°C
Bingham	$\tau = 10.550 + 0.075 \times \gamma$ $R^2 = 0.9413$, $F = 64.12$, $p = 0.0013$	$\tau = 10.794 + 0.096 \times \gamma$ $R^2 = 0.9547$, $F = 84.36$, $p = 0.008$	$\tau = 7.203 + 0.083 \times \gamma$ $R^2 = 0.9734$, $F = 146.39$, $p = 0.003$	$\tau = 4.591 + 0.067 \times \gamma$ $R^2 = 0.9801$, $F = 197.49$, $p = 0.001$
Power Law	$\tau = 1.567 \times \gamma^{0.570}$ $R^2 = 0.9988$, $F = 3226.91$, $p = 0.000$	$\tau = 1.306 \times \gamma^{0.629}$ $R^2 = 0.9929$, $F = 649.21$, $p = 0.000$	$\tau = 0.706 \times \gamma^{0.696}$ $R^2 = 0.9965$, $F = 1133.02$, p=0.000	$\tau = 0.377 \times \gamma^{0.754}$ $R^2 = 0.9931$, $F = 574.27$, $p = 0.000$
Carson	$\tau^{1/2} = 3.128^{1/2} + 0.058^{1/2} \times \gamma^{1/2}$ $R^2 = 0.9802$, $F = 198.00$, $p = 0.001$	$\tau^{1/2} = 2.990^{1/2} + 0.076^{1/2} \times \gamma^{1/2}$ $R^2 = 0.9859$, $F = 280.20$, $p = 0.001$	$\tau^{1/2} = 1.763^{1/2} + 0.068^{1/2} \times \gamma^{1/2}$ $R^2 = 0.9916$, $F = 473.76$, $p = 0.000$	$\tau^{1/2} = 1.180^{1/2} + 0.054^{1/2} \times \gamma^{1/2}$ $R^2 = 0.9941$, $F = 678.97$, $p = 0.000$
Herschel-Bulkley	$\tau = 0.576 + 1.684 \times \gamma^{0.560}$ $R^2 = 0.9988$, $F = 1267.45$, $p = 0.000$	$\tau = 0.328 + 1.261 \times \gamma^{0.634}$ $R^2 = 0.9939$, $F = 244.04$, $p = 0.005$	$\tau = 0.764 + 0.636 \times \gamma^{0.710}$ $R^2 = 0.9966$, $F = 441.39$, $p = 0.002$	$\tau = 0.953 + 0.317 \times \gamma^{0.777}$ $R^2 = 0.9935$, $F = 227.57$, $p = 0.005$

4.1. Physical Plugging of Nanoparticles. To shale featured with nanosized pores, nano-SiO_2 has a fair chance of plugging the pores and forms low permeability sealing zones. The plugging of nano-SiO_2 into shale had been confirmed by Sensoy et al. [23] who ran scanning electron microscope tests (Figure 9) on the Atoka shale in contact with 20 nm nano-SiO_2. It is difficult for nano-SiO_2 to plug all the pore throats; however, the average pore throats would decrease with the plugging of nano-SiO_2 into the pore throats, which would increase the capillary force and restrict the further invading of drilling mud (Figures 7 and 8). On the other side, the sealing zone formed by nano-SiO_2 is beneficial to form thinner mud cake and lower fluid loss of drilling mud, as shown in Figure 3. Furthermore, approximate spherical nano-SiO_2 can act as nanosized bearings in mud cakes, improve the lubricity of mud cakes, and reduce the frictional resistance of drilling bits and tools especially in horizontal wells for shale gas. As a whole, physical plugging of nano-SiO_2 can block the nanosized pore throats, restrict the transmission of pore pressure, and therefore improve wellbore stability.

4.2. Balanced Activity with Inorganic Salts. In case water activity of drilling mud is lower than that of the shale, osmotic pressure induced by the water activity difference can partially mitigate pressure transmission and fluid invasion from drilling mud into shale caused by hydraulic pressure. In the NPBMs, the addition of NaCl and KCl can decrease water activity of the drilling mud to form balanced activity drilling mud to shale formation.

4.3. Chemical Inhibition. Shale inhibitor Soltex was used in the NPBMs aiming at mitigating the water adsorption of shale. Plenty of ions with negative charge of Soltex can attach to the edge of ions with positive charge and restrict

water adsorption into shale. As one of the asphalt additives, Soltex can also squeeze into the possible micro fractures in shale driven by drilling mud pressure and improve the whole integrity of the wellbore. Additionally, other shale inhibitors and filtration additives as lockseal, SPNH, and SMP-II are beneficial to decrease fluid loss and further restrict the expansion and dispersion of shale and therefore improve wellbore stability.

4.4. Rational Drilling Mud Density. The pressure differential between drilling mud pressure and pore fluid pressure, which acts like a support pressure for the borehole, is a critical factor for wellbore stability. Too low mud density might cause overflow of pore fluid into the wellbore and even cause blowout of oil and gas while too high mud density would cause lost circulation and also speed up the invasion of fluid into shale. Generally, additional 0.1–0.2 g/cm^3 over pore fluid pressure is acceptable.

Basing on the physical plugging of nanoparticles, balanced activity with inorganic salts, chemical inhibition, and rational drilling mud density, a synergic wellbore stabilization theory was simply described as follows. First, attapulgite was used for it has excellent salt resistance thus improving the filtration property of the NPBMs. We also found that the mud had better thermal resistance and salt resistance when the proportion of attapulgite and bentonite was 1 : 1. Second, nano-SiO_2 had rather good thermal resistance at up to 180°C and can plug the nanosized pore throats existing in shale. It can also decrease fluid loss and improve the lubricity of the brine mud. Third, the addition of inorganic salts such as KCl and NaCl is helpful to lower water activity and to form balanced activity brine mud for shale. Fourth, powerfully chemical inhibition of Soltex can restrict water adsorption of shale. Fifth, in presence of proper portion of barite, mud density can be kept in a rational range to avoid wellbore instability or lost circulation. Finally, previous experiments showed that the recovery rate of gas permeability of coal samples was up to 72%–96% [25], indicating that the invasion of nano-SiO_2 was rather shallow which is beneficial for reservoir protection.

5. Conclusions

(1) The NPBMs embody excellent salt tolerance and thermal resistance for its rheological parameters did not suffer significant fluctuation. The NPBM-1 (4% NaCl plus 3% KCl) had a filtration of 7.6 mL at 180°C and the NPBM-2 (10% NaCl plus 3% KCl) had a filtration of 6.6 mL at 150°C.

(2) Rather low water activity and good lubricity of the NPBMs improve the mud systems' capability for wellbore stabilization and reduce circulation friction resistance.

(3) Pressure transmission tests on the NPBM-1 indicate that the system has perfect performances in mitigating or even preventing the transmission of drilling mud pressure into shale thus improving wellbore stability.

(4) Basing on the physical plugging of nanoparticles, balanced activity with inorganic salts, chemical inhibition, and rational drilling mud density, a synergic wellbore stabilization theory was simply proposed with the NPBMs.

(5) The optimal rheological models for the NPBM-1 and NPBM-2 were Herschel-Bulkley model and Power Law model separately.

Conflict of Interests

The authors declare that there is no conflict of interests regarding the publication of this paper.

Acknowledgments

The study is supported by the National Science Foundation of China (no. 41072111), the CNPC Innovation Foundation (no. 2014D-5006-0308), the Key Project of Natural Science Foundation of Hubei Province (no. 2015CFA135), and the Special Fund for Basic Scientific Research of Central Colleges (no. CUG130612).

References

[1] M. Lal, "Shale stability: drilling fluid interaction and shale strength," in *Proceedings of the SPE Asia Pacific Oil and Gas Conference and Exhibition*, Society of Petroleum Engineers, Jakarta, Indonesia, April 1999.

[2] R. P. Steiger and P. K. Leung, "Quantitative determination of the mechanical properties of shales," *SPE Drilling Engineering*, vol. 7, no. 3, pp. 181–185, 1992.

[3] E. Van Oort, D. Ripley, I. Ward, J. W. Chapman, R. Williamson, and M. Aston, "Silicate-based drilling fluids: competent, cost-effective and benign solutions to wellbore stability problems," in *Proceedings of the SPE/IADC Drilling Conference*, SPE 35059, New Orleans, La, USA, March 1996.

[4] M. E. Chenevert, "Shale control with balanced- activity oil-continuous muds," *Journal of Petroleum Technology*, vol. 22, no. 10, pp. 1309–1316, 1970.

[5] R. T. Ewy and E. K. Morton, "Wellbore-stability performance of water-based mud additives," *SPE Drilling and Completion*, vol. 24, no. 3, pp. 390–397, 2009.

[6] A. Hayatdavoudi and E. Apande, "A theoretical analysis of wellbrore failure and stability in shales," in *Proceedings of the 27th U.S. Symposium on Rock Mechanics (USRMS '86)*, ARMA-86-0571, Tuscaloosa, Ala, USA, June 1986.

[7] S. Carminati, L. Del Gaudio, and M. Brignoli, "Shale stabilisation by pressure propagation prevention," in *Proceedings of the SPE Annual Technical Conference and Exhibition*, SPE 63053, Dallas, Tex, USA, October 2000.

[8] P. I. Reid, B. Dolan, and S. Cliffe, "Mechanism of shale inhibition by polyols in water based drilling fluids," in *Proceedings of the SPE International Symposium on Oilfield Chemistry*, SPE-28960-MS, San Antonio, Tex, USA, February 1995.

[9] H. Zhong, Z. Qiu, W. Huang, and J. Cao, "Shale inhibitive properties of polyether diamine in water-based drilling fluid," *Journal of Petroleum Science and Engineering*, vol. 78, no. 2, pp. 510–515, 2011.

[10] T. M. Al-Bazali, J. Zhang, M. E. Chenevert, and M. M. Sharma, "Measurement of the sealing capacity of shale caprocks," in *Proceedings of the SPE Annual Technical Conference and Exhibition*, SPE-96100-MS, Dallas, Tex, USA, October 2005.

[11] P. H. Nelson, "Pore-throat sizes in sandstones, tight sandstones, and shales," *AAPG Bulletin*, vol. 93, no. 3, pp. 329–340, 2009.

[12] A. R. Joseph, H. R. Chad, D. C. Mery, I. Y. Akkutlu, and C. Sondergeld, "New pore-scale considerations for shale gas in place calculations," in *Proceedings of the SPE Unconventional Gas Conference*, SPE 131772, Pittsburgh, Pa, USA, February 2010.

[13] M. Milner, R. McLin, and J. Petriello, "Imaging texture and porosity in mudstones and shales: comparison of secondary and ion-milled backscatter SEM methods," in *Proceedings of the Canadian Unconventional Resources and International Petroleum Conference*, SPE 138975, Calgary, Canada, October 2010.

[14] J. Schieber, "Common themes in the formation and preservation of intrinsic porosity in shales and mudstones—illustrated with examples across the Phanerozoic," in *Proceedings of the SPE Unconventional Gas Conference*, SPE 132370, Pittsburgh, Pa, USA, February 2010.

[15] C. H. Sondergeld, R. J. Ambrose, C. S. Rai, and J. Moncrieff, "Micro-structural studies of gas shales," in *Proceedings of the SPE Unconventional Gas Conference*, SPE-131771-MS, Pittsburgh, Pa, USA, February 2010.

[16] C. Zou, R. Zhu, B. Bai et al., "First discovery of nano-pore throat in oil and gas reservoir in China and its scientific value," *Acta Petrologica Sinica*, vol. 27, no. 6, pp. 1857–1864, 2011.

[17] J. Cai, M. E. Chenevert, M. M. Sharma, and J. Friedheim, "Decreasing water invasion into Atoka shale using nonmodified silica nanoparticles," *SPE Drilling & Completion*, vol. 27, no. 1, pp. 103–112, 2012.

[18] M. M. Sharma, M. E. Chenevert, Q. Guo, L. Ji, J. Friedheim, and R. Zhang, "A new family of nanoparticle based drilling fluids," in *Proceedings of the SPE Annual Technical Conference and Exhibition*, SPE-160045, Society of Petroleum Engineers, San Antonio, Tex, USA, October 2012.

[19] S. Akhtarmanesh, M. J. A. Shahrabi, and A. Atashnezhad, "Improvement of wellbore stability in shale using nanoparticles," *Journal of Petroleum Science and Engineering*, vol. 112, pp. 290–295, 2013.

[20] P. P. Kapadnis, B. H. Ghansar, S. P. Mandan, and P. Pandey, "Thermoelectric nanomaterial: a demiurgic approach towards improvement of shale stability," in *Proceedings of the SPE Unconventional Gas Conference and Exhibition*, SPE-164000-MS, Muscat, Oman, January 2013.

[21] C. Liang, M. Chen, B. Lu et al., "The study of nano sealing to improve the brittle shale wellbore stability under dynamic load," in *Proceedings of the Offshore Technology Conference-Asia*, OTC-24919-MS, Kuala Lumpur, Malaysia, March 2014.

[22] Y. Yuan, J. Cai, J. Wang, and C. Xiao, "Experimental study on improving filtration properties of drilling fluid using silica nano-particles," *Oil Drilling & Production Technology*, vol. 35, no. 3, pp. 30–41, 2013.

[23] T. Sensoy, M. E. Chenevert, and M. M. Sharma, "Minimizing water invasion in shales using nanoparticles," in *Proceedings of the SPE Annual Technical Conference and Exhibition*, SPE-124429-MS, New Orleans, La, USA, October 2009.

[24] F. K. Mody, U. A. Tare, C. P. Tan, C. J. Drummond, and B. Wu, "Development of novel membrane efficient water-based drilling fluids through fundamental understanding of osmotic membrane generation in shales," in *Proceedings of the SPE Annual Technical Conference and Exhibition*, SPE 77447, San Antonio, Tex, USA, September 2002.

[25] J.-H. Cai, Y. Yuan, J.-J. Wang, X.-J. Li, and W.-J. Cao, "Experimental research on decreasing coalbed methane formation damage using micro-foam mud stabilized by nanoparticles," *Journal of the China Coal Society*, vol. 38, no. 9, pp. 1640–1645, 2013.